Mon. Not. R. Astron. Soc. **378,** 1165–1176 (2007) doi:10.1111/j.1365-2966.2007.11851.x

Proper motion dispersions of red clump giants in the galactic bulge: observations and model comparisons

Nicholas J. Rattenbury,[1⋆] Shude Mao,[1⋆] Victor P. Debattista,[2⋆] Takahiro Sumi,[3⋆] Ortwin Gerhard[4⋆] and Flavio De Lorenzi[4⋆]

[1]*University of Manchester, Jodrell Bank Observatory, Macclesfield, Cheshire SK11 9DL*
[2]*Astronomy Department, University of Washington, Box 351580, Seattle, WA 98195-1580, USA*
[3]*Solar–Terrestrial Environment Laboratory, Nagoya University, Furo-cho, Chikusa-ku, Nagoya 464-8601, Japan*
[4]*Max-Planck-Institut fuer extraterrestrische Physik, PO Box 1312, D-85741 Garching, Germany*

Accepted 2007 April 12. Received 2007 April 10; in original form 2006 November 21

ABSTRACT

Red clump giants (RCGs) in the Galactic bulge are approximate standard candles and hence they can be used as distance indicators. We compute the proper motion dispersions of RCG stars in the Galactic bulge using the proper motion catalogue from the second phase of the Optical Gravitational Microlensing Experiment (OGLE-II) for 45 fields. The proper motion dispersions are measured to a few per cent accuracy due to the large number of stars in the fields. The observational sample comprises 577 736 stars. These observed data are compared to a state-of-the-art particle simulation of the Galactic bulge region. The predictions are in rough agreement with observations, but appear to be too anisotropic in the velocity ellipsoid. We note that there is significant field-to-field variation in the observed proper motion dispersions. This could either be a real feature, or due to some unknown systematic effect.

Key words: gravitational lensing – Galaxy: bulge – Galaxy: centre – Galaxy: kinematics and dynamics – Galaxy: structure.

1 INTRODUCTION

Many lines of evidence suggest the presence of a bar at the Galactic Centre, such as infrared maps (Dwek et al. 1995; Binney, Gerhard & Spergel 1997) and star counts (Nikolaev & Weinberg 1997; Stanek et al. 1997; Unavane & Gilmore 1998), see Gerhard (2002) for a review. However, the bar parameters are not well determined. For example, recent infrared star counts collected by the *Spitzer Space Telescope* are best explained assuming a bar at a $\sim 44^\circ$ angle to the Sun–Galactic Centre line (Benjamin et al. 2005) while most previous studies prefer a bar at $\sim 20^\circ$. In addition, there may be some fine features, such as a ring in the Galactic bulge, which are not yet firmly established (Babusiaux & Gilmore 2005). It is therefore crucial to obtain as many constraints as possible in order to better understand the structure of the inner Galaxy.

Many microlensing groups monitor the Galactic bulge, including the EROS (Aubourg et al. 1993), MACHO (Alcock et al. 2000), MOA (Bond et al. 2001; Sumi et al. 2003a) and Optical Gravitational Microlensing Experiment (OGLE) (Udalski et al. 2000) collaborations. In addition to discovering microlensing events, these groups have also accumulated a huge amount of data about the stars in the Galactic bulge spanning several years to a decade and a half.

Eyer & Woźniak (2001) first demonstrated that the data can be used to infer the proper motions of stars, down to $\sim$ mas yr^{-1}. Sumi et al. (2004) obtained the proper motions for millions of stars in the OGLE-II data base for a large area of the sky. In this paper, we focus on the red clump giants (RCGs). These stars are bright and they are approximately standard candles, hence their magnitudes can be taken as a crude measure of their distances. As the OGLE-II proper motions are relative, in this paper we compute the proper motion dispersions of bulge stars for all field data presented by Sumi et al. (2004), as they are independent of the unknown proper motion zero-points. These results could aid theoretical modelling efforts for the central regions of the Galaxy.

The structure of this paper is as follows. In Section 2, we describe the OGLE-II proper motion catalogue and compute the proper motion dispersions for bulge stars in 45 OGLE-II fields. In Section 3 we describe the stellar dynamical model of the Galaxy used in this work and detail how the model was used to generate proper motion dispersions. These model predictions are compared to the observational results in Section 4 and in Section 5 we discuss the implications of the results.

2 OBSERVED PROPER MOTION DISPERSIONS

The second phase of the OGLE experiment observed the Galactic Centre in 49 fields using the 1.3-m Warsaw telescope at the Las

⋆E-mail: nicholas.rattenbury@manchester.ac.uk (NJR); smao@jb.man.ac.uk (SM); debattis@astro.washington.edu (VPD); sumi@stelab.nagoya-u.ac.jp (TS); gerhard@exgal.mpe.mpg.de (OG); lorenzi@exgal.mpe.mpg.de (FDL)

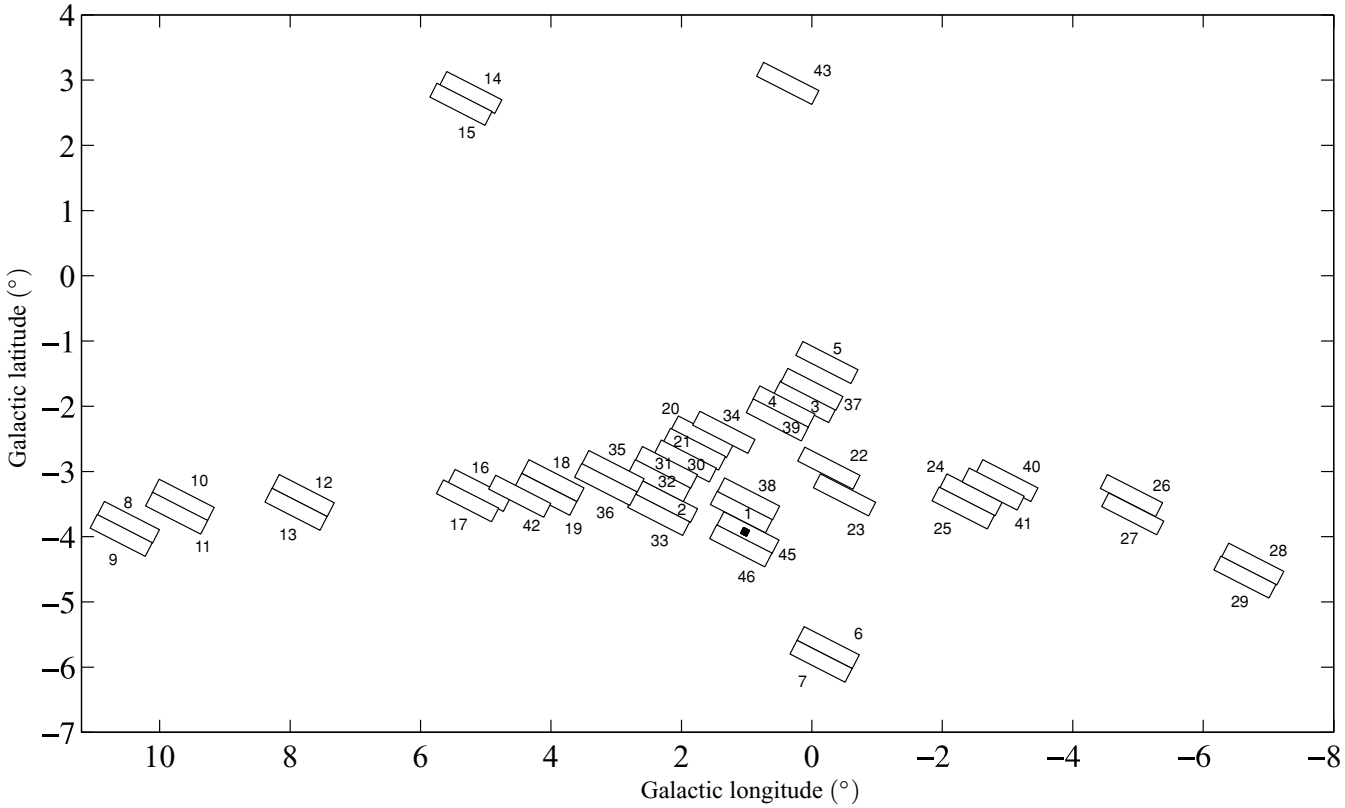

Figure 1. The position of the 45 OGLE-II fields used in this analysis. The field used in Spaenhauer et al. (1992) is shown, located within OGLE-II field 45 with $(l, b) = (1.^{\circ}0245, -3.^{\circ}9253)$.

Campanas Observatory, Chile. Data were collected over an interval of almost four years, between 1997 and 2000. Each field is 0.24×0.95 deg^2 in size. Fig. 1 shows the position of the OGLE-II Galactic bulge fields which returned data used in this paper.

2.1 Red clump giants

The RCGs are metal-rich horizontal branch stars (Stanek et al. 2000, and references therein). Theoretically, one expects their magnitudes to have (small) variations with metallicity, age and initial stellar mass (Girardi & Salaris 2001). Empirically they appear to be reasonable standard candles in the *I* band with little dependence on metallicities (Udalski 2000; Zhao, Qiu & Mao 2001). Below we describe the selection of RCG stars in more detail.

2.2 OGLE-II proper motion data

Bulge RCG stars are selected from the OGLE-II proper motion catalogue by applying a cut in magnitude and colour to all stars in each of the OGLE-II fields. We corrected for extinction and reddening using the maps presented by Sumi (2004) for each field. Stars were selected which are located in an ellipse with centre $(V - I)_0 = 1.0$, $I_0 = 14.6$; and semimajor (magnitude) and semiminor (colour) axes of 0.9 and 0.4, respectively, see Fig. 2; a similar selection criterion was used by Sumi (2004). Stars with errors in proper motion greater than 1 mas yr^{-1} in either the *l* or *b* directions were excluded. Stars with total proper motion greater than 10 mas yr^{-1} where similarly excluded, as these are likely to be nearby disc stars, see also Section 3.2. Fields 44, 47–49 were not analysed due to the low number of RCG stars appearing in these fields.

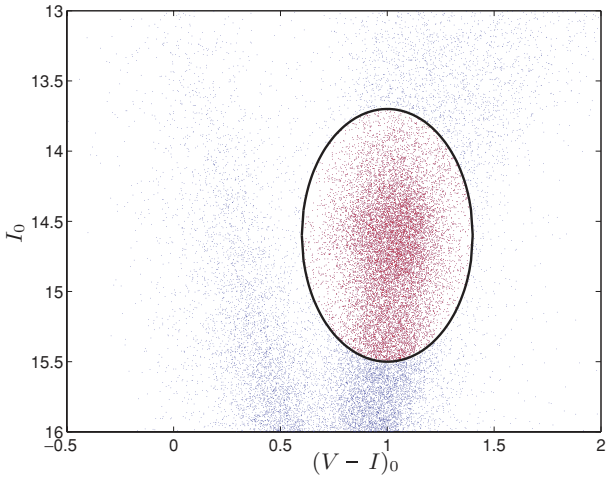

Figure 2. Extinction-corrected CMD for stars in the OGLE-II field 1. The ellipse defines the selection criteria for RCG stars based on colour and magnitude, see text. Sample stars are also required to have proper motion errors $s_{l,b} < 1$ mas yr^{-1} and total proper motion $\mu < 10$ mas yr^{-1}.

The proper motion dispersions for the longitude and latitude directions (σ_l and σ_b) were computed for each field via a maximum likelihood analysis following Lupton, Gunn & Griffin (1987). Assuming a Gaussian distribution of proper motions with mean $\bar{\mu}$ and intrinsic proper motion dispersion σ, the probability of a single observed proper motion μ_i with measurement error ξ_i is

$$p_i = \frac{1}{\sqrt{2\pi(\sigma^2 + \xi_i^2)}} \exp\left[-\frac{(\mu_i - \bar{\mu})^2}{2(\sigma^2 + \xi_i^2)}\right]. \quad (1)$$

Maximizing the likelihood $\ln(L) = \ln(\Pi\, p_i)$ for $\bar{\mu}$ and σ over all observations we find

$$\frac{\partial \ln L}{\partial \bar{\mu}} = \sum_i \frac{(\mu_i - \bar{\mu})}{\sigma^2 + \xi_i^2} = 0 \tag{2}$$

$$\Rightarrow \bar{\mu} = \sum_i \frac{\mu_i}{\sigma^2 + \xi_i^2} \Bigg/ \sum_i \left(\sigma^2 + \xi_i^2\right)^{-1} \tag{3}$$

and

$$\frac{\partial \ln L}{\partial \sigma} = \sum_i \frac{1}{\sigma^2 + \xi_i^2} - \sum_i \frac{(\mu_i - \bar{\mu})^2}{\left(\sigma^2 + \xi_i^2\right)^2} = 0 \tag{4}$$

which can be solved numerically to find σ^2.

The values of $\bar{\mu}$ and σ obtained using the above maximum likelihood analysis are virtually identical to those obtained via the equations in Spaenhauer, Jones & Whitford (1992). The errors on the observed proper motion dispersion values were determined from a bootstrap analysis using 500 samplings of the observed data set.

2.3 Extinction

In order to ensure the correction for extinction and reddening above does not affect the kinematic measurements, σ_l and σ_b were recomputed for each OGLE-II field using reddening-independent magnitudes. Following Stanek et al. (1997) we define the reddening-independent magnitude I_{V-I}:

$$I_{V-I} = I - \frac{A_I}{A_V - A_I}\,(V - I)\,, \tag{5}$$

where A_I and A_V are the extinctions in the I and V bands determined by Sumi (2004). The position of the red clump in the I_{V-I}, $(V - I)$ colour–magnitude diagram (CMD) varies from field to field. The red clump stars were extracted by iteratively applying a selection ellipse computed from the moments of the data (Rocha et al. 2002) rather than centred on a fixed colour and magnitude. The selection ellipse was recomputed iteratively for each sample until convergence. The proper motion dispersions σ_l and σ_b computed using RCG stars selected in this way are consistent with those determined using the original selection criteria on corrected magnitudes and colours.

2.4 Results

Table 1 lists the observed proper motion dispersions along with errors for each of the 45 OGLE-II fields considered in this paper.

Figs 3 and 4 show the proper motion dispersions σ_l and σ_b as a function of Galactic longitude and latitude. A typical value of σ_l or σ_b of 3.0 mas yr^{-1} corresponds to $\sim$110 km s^{-1}, assuming a distance to the Galactic Centre of 8 kpc. The proper motion dispersion profiles as a function of Galactic longitude shows some slight asymmetry about the Galactic Centre. This asymmetry may be related to the tri-axial Galactic bar structure (Stanek et al. 1997; Babusiaux & Gilmore 2005; Nishiyama et al. 2005). The most discrepant points in Fig. 3 correspond to the low-latitude field numbers 6 and 7 (see Fig. 1). The varying field latitude accounts for some of the scatter in Fig. 3, however we note below in Section 4.1 that there are significant variations in the observed proper motion dispersion between some pairs of adjacent fields. Owing to the lack of fields at positive Galactic latitude, any asymmetry about the Galactic Centre in the proper motion dispersions as a function of Galactic latitude is not obvious, see Fig. 4. Field-to-field variations in the proper motion dispersions similarly contribute to the scatter seen in Fig. 4, along with the wide range of field longitudes, especially for fields with $-4^\circ < b < -3^\circ$.

Koztowski et al. (2006) were the first to establish the presence of a detectable cross-correlation term in the velocity field of the Galactic bulge. Table 2 lists the proper motion dispersions and cross-correlation term C_{lb} in the OGLE-II Baade's Window (BW) fields 45 and 46 along with those found by Kozłowski et al. (2006) using *Hubble Space Telescope* (*HST*) data in four BW fields. The two sets of proper motion dispersions results are consistent at the $\sim 2\sigma$ level. It is important to note that the errors on the proper motion dispersions in Table 1 do not include systematic errors. We also note that the selection criteria applied to stars in the *HST* data are very different from those for the ground-based data, in particular the magnitude limits applied in each case. The bulge kinematics from the *HST* data of Kozłowski et al. (2006) were determined for stars with magnitudes $18.0 < I_{F814W} < 21.5$. The approximate reddening-independent magnitude range for the OGLE-II data was $12.5 \lesssim I_{V-I} \lesssim 14.6$. The effects of blending are also very different in the two data sets. It is therefore very reassuring that our results are in general agreement with those obtained by Kozłowski et al. (2006) using higher resolution data from the *HST*. For more comparisons between ground and *HST* RCG proper motion dispersions, see Section 4.

Fig. 5 shows the cross-correlation term C_{lb} as a function of Galactic coordinate. There is a clear sinusoidal structure in the C_{lb} data as a function of Galactic longitude, with the degree of correlation between σ_l and σ_b changing most rapidly near $l \simeq 0^\circ$. The C_{lb} data as a function of Galactic latitude may also show some evidence of structure. It is possible however, that this apparent structure is due to the different number of fields at each latitude, rather than some real physical cause.

3 GALACTIC MODEL

The stellar dynamical model used in this work was produced using the made-to-measure method (Syer & Tremaine 1996). The model is constrained to reproduce the density distribution constructed from the dust-corrected L-band *COBE*/DIRBE map of Spergel, Malhotra & Blitz (1996). An earlier dynamical model was built to match the total column density of the disc (Bissantz & Gerhard 2002). This dynamical model matched the radial velocity and proper motion data in two fields (including BW) quite well. No kinematic constraints were imposed during the construction of the model. We refer the readers to Bissantz, Debattista & Gerhard (2004) for more detailed descriptions. The model used here is constructed as in that case with the further refinement that the vertical density distribution is also included. This is necessary as the vertical kinematics (σ_b) will also be compared with observations in this paper. However, the density distribution near the mid-plane is considerably more uncertain, in part because of the dust-extinction correction. Thus the model used in this paper can only be considered illustrative, not final. Further efforts to model the vertical density distribution are currently under way and will be reported elsewhere (Debattista et al., in preparation).

In Fig. 6, we present the mean motion of stars in the mid-plane of the Galaxy from this model. A bar position angle of $\theta = 20^\circ$ is shown here, as this is the orientation favoured both by optical depth measurements (Evans & Belokurov 2002) and by the RCG brightness distribution (Stanek et al. 1997) and was the angle used in deriving the model. Clearly, one can see that the mean motion follows elliptical paths around the Galactic bar. The analysis of OGLE-II proper

Table 1. Observed proper motion (PM) dispersions in the longitude and latitude directions, σ_l, σ_b, and cross-correlation term C_{lb} for bulge stars in 45 OGLE-II fields. High-precision proper motion data for bulge stars were extracted from the OGLE-II proper motion catalogue (Sumi et al. 2004). N is the number of stars selected from each field. Fields 44, 47–49 were not analysed due to the low number of RCG stars appearing in these fields.

Field	Field centre		PM dispersions (mas yr^{-1})		C_{lb}	N
	$l(^\circ)$	$b(^\circ)$	Longitude σ_l	Latitude σ_b		
1	1.08	−3.62	3.10 ± 0.02	2.83 ± 0.02	−0.13 ± 0.01	15 434
2	2.23	−3.46	3.21 ± 0.02	2.80 ± 0.02	−0.14 ± 0.01	16 770
3	0.11	−1.93	3.40 ± 0.01	3.30 ± 0.02	−0.08 ± 0.01	26 763
4	0.43	−2.01	3.43 ± 0.02	3.26 ± 0.01	−0.11 ± 0.01	26 382
5	−0.23	−1.33	3.23 ± 0.03	3.00 ± 0.04	−0.04 ± 0.02	3145
6	−0.25	−5.70	2.61 ± 0.02	2.36 ± 0.03	−0.06 ± 0.01	7027
7	−0.14	−5.91	2.70 ± 0.03	2.43 ± 0.02	−0.05 ± 0.01	6236
8	10.48	−3.78	2.80 ± 0.03	2.29 ± 0.02	−0.08 ± 0.01	5136
9	10.59	−3.98	2.73 ± 0.02	2.16 ± 0.03	−0.06 ± 0.01	5114
10	9.64	−3.44	2.77 ± 0.02	2.27 ± 0.02	−0.07 ± 0.01	5568
11	9.74	−3.64	2.84 ± 0.02	2.32 ± 0.02	−0.10 ± 0.01	5369
12	7.80	−3.37	2.66 ± 0.03	2.31 ± 0.03	−0.08 ± 0.01	6035
13	7.91	−3.58	2.66 ± 0.03	2.24 ± 0.02	−0.07 ± 0.01	5601
14	5.23	2.81	2.97 ± 0.02	2.60 ± 0.02	0.04 ± 0.01	10 427
15	5.38	2.63	3.02 ± 0.02	2.64 ± 0.03	−0.00 ± 0.01	8989
16	5.10	−3.29	2.87 ± 0.02	2.53 ± 0.02	−0.12 ± 0.01	9799
17	5.28	−3.45	2.81 ± 0.02	2.42 ± 0.01	−0.12 ± 0.01	10 268
18	3.97	−3.14	2.92 ± 0.02	2.62 ± 0.02	−0.13 ± 0.01	14 019
19	4.08	−3.35	2.90 ± 0.02	2.60 ± 0.02	−0.17 ± 0.01	13 256
20	1.68	−2.47	3.27 ± 0.01	2.82 ± 0.01	−0.12 ± 0.01	17 678
21	1.80	−2.66	3.31 ± 0.02	2.90 ± 0.02	−0.13 ± 0.01	17 577
22	−0.26	−2.95	3.17 ± 0.02	2.84 ± 0.02	−0.01 ± 0.01	19 787
23	−0.50	−3.36	3.15 ± 0.01	2.84 ± 0.02	−0.04 ± 0.01	17 996
24	−2.44	−3.36	2.96 ± 0.01	2.48 ± 0.01	0.02 ± 0.01	16 397
25	−2.32	−3.56	2.91 ± 0.01	2.50 ± 0.01	0.02 ± 0.01	16 386
26	−4.90	−3.37	2.68 ± 0.02	2.17 ± 0.01	0.02 ± 0.01	13 099
27	−4.92	−3.65	2.63 ± 0.02	2.15 ± 0.01	0.03 ± 0.01	12 728
28	−6.76	−4.42	2.63 ± 0.03	2.12 ± 0.02	−0.01 ± 0.01	8367
29	−6.64	−4.62	2.66 ± 0.03	2.09 ± 0.02	−0.02 ± 0.01	8108
30	1.94	−2.84	3.04 ± 0.02	2.70 ± 0.02	−0.12 ± 0.01	17 774
31	2.23	−2.94	3.11 ± 0.02	2.74 ± 0.01	−0.12 ± 0.01	17 273
32	2.34	−3.14	3.10 ± 0.02	2.78 ± 0.01	−0.13 ± 0.01	15 966
33	2.35	−3.66	3.08 ± 0.02	2.77 ± 0.02	−0.14 ± 0.01	15 450
34	1.35	−2.40	3.36 ± 0.02	2.92 ± 0.01	−0.11 ± 0.01	16 889
35	3.05	−3.00	3.09 ± 0.02	2.72 ± 0.02	−0.14 ± 0.01	15 973
36	3.16	−3.20	3.19 ± 0.02	2.77 ± 0.02	−0.16 ± 0.01	14 955
37	0.00	−1.74	3.29 ± 0.02	3.04 ± 0.01	−0.05 ± 0.01	20 233
38	0.97	−3.42	3.15 ± 0.01	2.84 ± 0.02	−0.12 ± 0.01	15 542
39	0.53	−2.21	3.21 ± 0.01	3.00 ± 0.01	−0.07 ± 0.01	24 820
40	−2.99	−3.14	2.84 ± 0.01	2.47 ± 0.02	0.05 ± 0.01	13 581
41	−2.78	−3.27	2.78 ± 0.01	2.41 ± 0.02	0.04 ± 0.01	14 070
42	4.48	−3.38	2.89 ± 0.02	2.63 ± 0.02	−0.15 ± 0.01	10 099
43	0.37	2.95	3.17 ± 0.02	2.87 ± 0.01	0.02 ± 0.01	11 467
45	0.98	−3.94	2.97 ± 0.04	2.61 ± 0.04	−0.13 ± 0.02	2380
46	1.09	−4.14	2.90 ± 0.04	2.67 ± 0.04	−0.16 ± 0.03	1803

motions by Sumi, Eyer & Woźniak (2003b) is consistent with this streaming motion.

3.1 Model stellar magnitudes

The model has a four-fold symmetry, obtained by a rotation of π radians around the vertical axis and by positioning the Sun above or below the mid-plane. The kinematics of model particles falling within the solid angle of each OGLE-II field were combined to those from the three other equivalent lines of sight. This procedure allows an increase in the number of model particles used for the predictions of stellar kinematics.

We assign magnitudes to stars in the Galactic model described above which appear in the same fields as that observed by the OGLE collaboration. Number counts as a function of I-band apparent magnitude, I, were used to compute the fraction of RCG stars in each of the OGLE-II fields. Fig. 7 shows an example of the fitted number count function $N_k(I)$ for one of the $k = 1$–49 OGLE-II fields, where $N_k(I)$ is of the form of a power law and a Gaussian (Sumi 2004):

$$N_k(I) = a_k 10^{(b_k I)} + c_k \exp\left[\frac{-(I - I_{p,k})^2}{2\sigma_k^2}\right], \quad (6)$$

where the constants $a_k, b_k, c_k, I_{p,k}, \sigma_k$ are determined for each of the

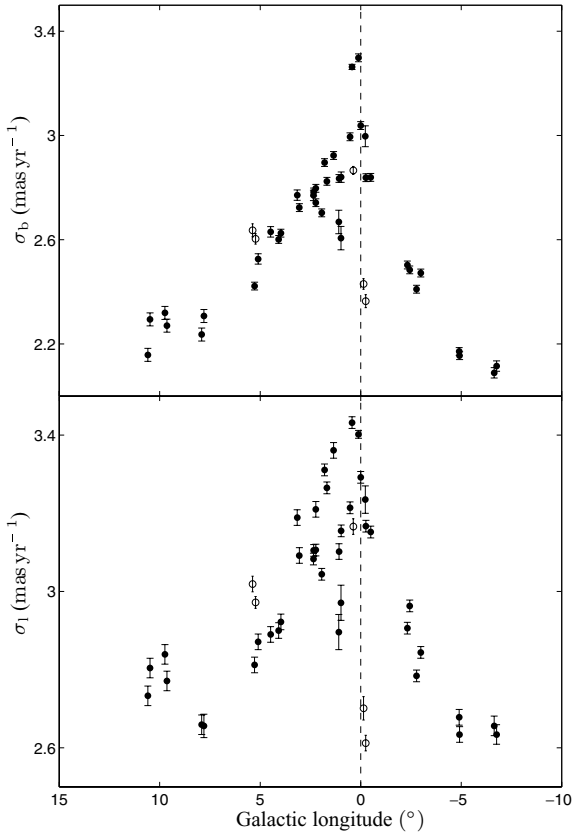

Figure 3. Proper motion dispersion in the Galactic longitude (σ_l) and latitude (σ_b) directions for 45 OGLE-II Galactic bulge fields as a function of field Galactic longitude. Open circles correspond to fields 6, 7, 14, 15 and 43 which have relatively extreme galactic latitudes, see Fig. 1.

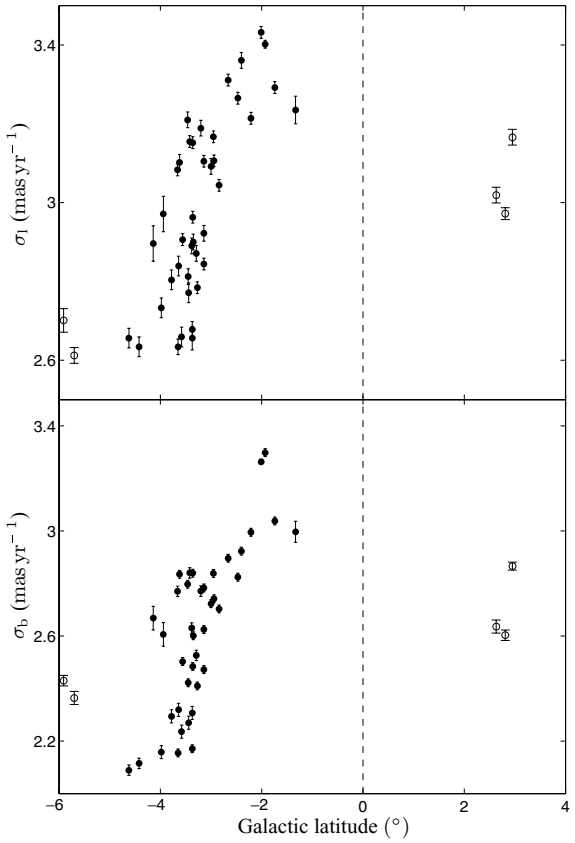

Figure 4. Proper motion dispersion in the Galactic longitude (σ_l) and latitude (σ_b) directions for 45 OGLE-II Galactic bulge fields as a function of field Galactic latitude. Open circles correspond to fields 6, 7, 14, 15 and 43 which have relatively extreme galactic latitudes, see Fig. 1.

k OGLE-II fields, see Table 3. The fraction R_k of RCG stars is evaluated as the ratio of the area under the Gaussian component of equation (6) to the area under the full expression. The integrals are taken over $\pm 3\sigma_k$ around the RCG peak in $N_k(I)$ for each of the k OGLE-II fields. Fields 44 and 47–49 are not included as there are insufficient RCGs in the OGLE-II fields to fit equation (6). Fig. 7 shows that the model number count function fails to fit the observed number counts well for magnitudes $I \simeq 15.4$. In order to convert stellar density to a distribution of apparent magnitude, the relevant quantity is ρr^3 (Bissantz & Gerhard 2002). Depending on the line of sight, this quantity can give asymmetric magnitude distributions through the bulge. Using the best-fitting analytic tri-axial density models for the bulge (Rattenbury et al. 2007), this asymmetry is observed and may explain the excess of stars in the number count histograms, compared to the best-fitting two-component fit of equation (6). The inability of equation (6) to model completely all features in the observed number counts in some cases leads to an additional uncertainty in the magnitude location of the fitted Gaussian peak. Computing the apparent magnitude distribution as $\propto \rho r^3$ also produces a small shift in the peak of the magnitude distribution. This shift is $\sim +0.04$ mag for $l = 0^\circ, b = 0^\circ$. The proper motion dispersions computed here are unlikely to be sensitive to these small offsets.

Each star in the Galactic model is assigned an RCG magnitude with probability R_k for each field. The apparent magnitude is computed using the model distance. Stars which are not assigned an RCG magnitude are assigned a magnitude using the power-law component of equation (6), defined over the same limits used to compute R_k. Here we implicitly assume that the RCG stars trace the overall Galactic disc and bulge populations.

The RCG luminosity function is approximated by a Gaussian distribution with mean magnitude -0.26 and $\sigma = 0.2$. These assumptions are mostly consistent with observations (Stanek et al. 1997) and the fitted distribution from Udalski (2000), but there may be small offsets between local and bulge RCGs. It was noted in Sumi (2004) that there is some as-yet unexplained offset (0.3 mag) in the extinction-corrected mean RCG magnitudes in the OGLE fields. A possible explanation for this offset is that the RCG population effects are large, so that the absolute magnitude of RCG stars is significantly different for RCGs in the bulge compared to local RCGs, as claimed by Percival & Salaris (2003) and Salaris et al. (2003). A different value of the distance to the Galactic Centre to that assumed here (8 kpc) would in part account for the discrepancy, however would not remove it completely. Using a value of 7.6 kpc (Eisenhauer et al. 2005; Nishiyama et al. 2006) as the distance to the Galactic Centre would change the zero-point by 0.12 mag, resulting in an offset value of 0.18 mag. It is also possible that reddening towards the Galactic Centre is more complicated than assumed in Sumi (2004). In order to compare the model proper motion results with the observed data, it was necessary to shift the mean model RCG magnitudes to correspond to that observed in each of the OGLE fields. The model RCG magnitudes were fitted with a Gaussian curve. The mean of the model RCG magnitudes was then shifted by a value Δm, see Table 3, to correspond to the observed

Table 2. Comparison between proper motion dispersions and cross-correlation term $C_{\rm lb}$ in two of the OGLE-II fields (45 and 46) with proper motion dispersions computed from four nearby *HST* fields (Kozłowski et al. 2006).

Field	$l(^\circ)$	$b(^\circ)$	$\sigma_{\rm l}$ (mas yr^{-1})	$\sigma_{\rm b}$ (mas yr^{-1})	$C_{\rm lb}$	Reference
119-A	1.32	−3.77	2.89 ± 0.10	2.44 ± 0.08	-0.14 ± 0.04	1
119-C	0.85	−3.89	2.79 ± 0.10	2.65 ± 0.08	-0.14 ± 0.04	1
OGLE-II 45	0.98	−3.94	2.97 ± 0.04	2.61 ± 0.04	-0.13 ± 0.02	2
119-D	1.06	−4.12	2.75 ± 0.10	2.56 ± 0.09	-0.05 ± 0.06	1
95-BLG-11	0.99	−4.21	2.82 ± 0.09	2.62 ± 0.09	-0.14 ± 0.04	1
OGLE-II 46	1.09	−4.14	2.90 ± 0.04	2.67 ± 0.04	-0.16 ± 0.03	2

(1) Kozłowski et al. (2006); (2) this work.

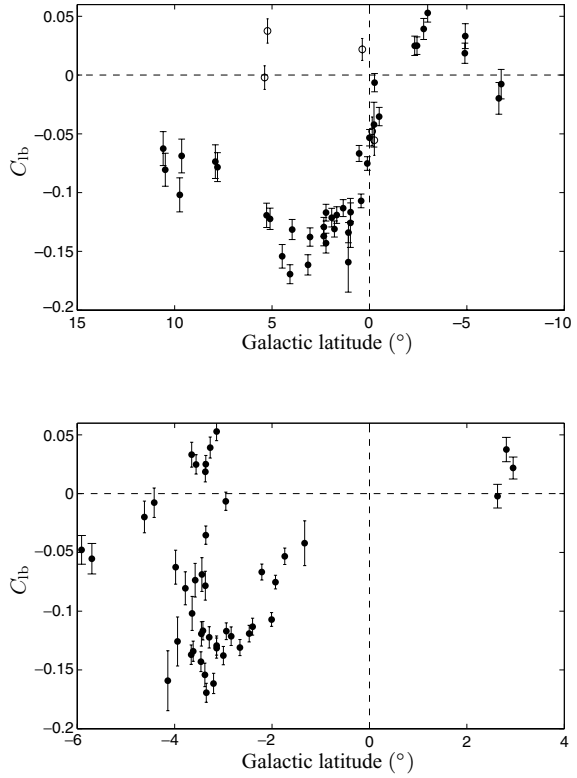

Figure 5. Cross-correlation term $C_{\rm lb}$ for 45 OGLE-II Galactic bulge fields as a function of field Galactic longitude (top) and latitude (bottom). Open circles in the top plot of $C_{\rm lb}$ versus l correspond to fields 6, 7, 14, 15 and 43 which have relatively extreme galactic latitudes, see Fig. 1.

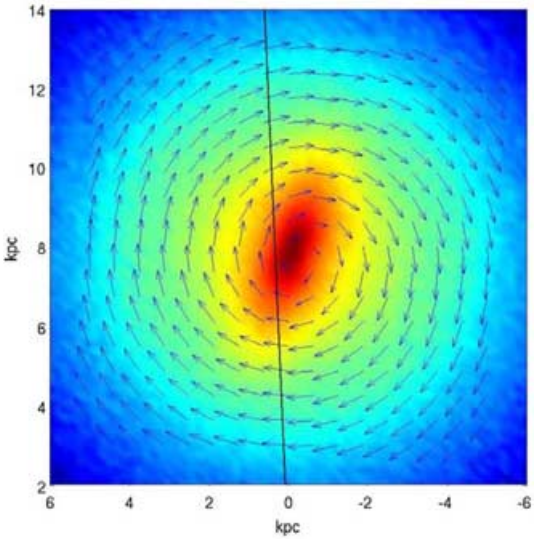

Figure 6. Galactic kinematics from the model of Debattista et al. (in preparation). Bulk stellar motion in the mid-plane of the Galaxy is shown superimposed on the stellar density. The Sun is located at the origin (not shown). An example line of sight is shown. The model can be rotated to four equivalent positions for each line of sight due to symmetry (see Section 3.1).

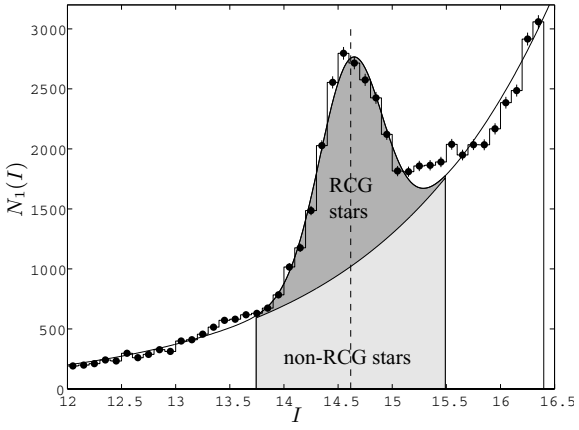

Figure 7. Number count as function of apparent magnitude, I, for OGLE-II field 1. The number count histogram is shown along with the fitted function equation (6). The fraction of RCG stars, R_k, is evaluated over the magnitude range $I_{\rm p} \pm 3\sigma$ for each of the (k = 1–49) OGLE-II fields. The ratio R_k is assumed to be the same at all stellar distances for each field.

mean RCG magnitude in each of the OGLE fields. Note that we concentrate on second-order moments (proper motion dispersions) of the proper motion, so a small shift in the zero-point has little effect on our results.

Every model particle has an associated weight, w_i. The particle weight can take values $0 < w_i \lesssim 20$. In order to account for this weighting, $\lceil w_i \rceil$ stars are generated for each particle with the same kinematics but magnitudes determined as above. $\lceil w_i \rceil$ is the nearest integer towards $+\infty$. Each model star is then assigned a weight, $\gamma_i = w_i/\lceil w_i \rceil$. Note that this procedure allows us to increase the effective number of particles to better sample the luminosity function. The total number of stars and the number of stars assigned RCG magnitudes in each field are listed in Table 3 as $n_{\rm all}$ and $n_{\rm rcg}$, respectively. 81 806 stars from the model were used to compare model kinematics to observed values.

Table 3. Values of fitted parameters in equation (6) for all 45 OGLE-II fields used in this analysis. R is the ratio of observed RCG stars to the total number of stars in each field, evaluated over $\pm 3\sigma$ around the RCG peak magnitude, I_p, where σ is the fitted Gaussian spread in equation (6). The magnitudes of the model RCG stars are shifted by Δm to correspond to the observed mean RCG magnitude in each field. The total number of model stars in each field-assigned RCG magnitudes and colours is n_{rcg} and the total number of model stars in each field is n_{all}. The corresponding total model weight values for each field are given by w_{rcg} and w_{all}, respectively. The large values of σ for fields 8–11 might be related to their position at large positive longitudes, and could indicate a structure such as the end of the bar, a ring or spiral arm. An analysis of the bar morphology based on these results is underway (Rattenbury et al. 2007).

Field	a	b	c	I_p	σ	R	Δm	n_{rcg}	n_{all}	w_{rcg}	w_{all}
1	0.11	0.27	1735.70	14.62	0.29	0.40	0.43	585	1773	277.2	842.4
2	0.15	0.26	1876.47	14.54	−0.29	0.43	0.41	621	1802	298.1	853.9
3	0.16	0.28	4692.78	14.66	0.25	0.44	0.54	1264	3626	668.5	1911.1
4	0.17	0.28	4438.63	14.65	0.24	0.44	0.52	1298	3653	670.8	1922.2
5	0.05	0.33	4581.59	14.70	0.28	0.33	0.55	1342	4668	755.7	2685.7
6	0.04	0.27	519.71	14.57	0.37	0.34	0.36	152	583	69.5	270.8
7	0.03	0.28	457.42	14.55	0.39	0.32	0.36	143	527	71.9	243.8
8	0.04	0.27	259.65	14.37	−0.51	0.22	0.35	96	561	41.7	236.2
9	0.04	0.27	270.90	14.34	0.51	0.25	−0.05	96	497	46.1	230.9
10	0.08	0.26	321.32	14.44	0.52	0.22	0.40	131	654	49.1	260.1
11	0.04	0.28	316.25	14.45	0.50	0.23	0.28	128	695	57.5	339.4
12	0.12	0.25	546.85	14.43	0.38	0.28	0.41	238	908	100.7	393.1
13	0.10	0.25	520.45	14.45	0.37	0.29	0.15	190	863	83.9	392.4
14	0.09	0.28	1309.28	14.55	0.32	0.35	0.34	458	1587	216.0	767.4
15	0.05	0.29	1154.52	14.57	0.33	0.31	0.55	421	1661	185.2	761.8
16	0.12	0.27	1042.72	14.50	0.35	0.33	0.50	397	1383	172.8	601.1
17	0.12	0.26	1069.07	14.48	0.34	0.35	0.25	406	1443	212.4	753.4
18	0.17	0.26	1569.83	14.49	0.31	0.40	0.35	527	1564	234.7	702.4
19	0.17	0.26	1429.23	14.51	0.32	0.40	0.44	434	1365	184.4	608.5
20	0.20	0.27	3012.09	14.58	0.26	0.42	0.53	939	2728	480.3	1398.3
21	0.15	0.27	2793.36	14.58	0.26	0.43	0.45	900	2554	443.5	1260.0
22	0.12	0.28	2574.77	14.74	0.28	0.42	0.51	830	2419	382.5	1113.3
23	0.09	0.28	2147.71	14.73	0.29	0.42	0.47	767	2126	384.2	1060.6
24	0.12	0.27	2130.41	14.82	0.28	0.42	0.50	595	1864	269.6	905.4
25	0.07	0.28	2002.91	14.82	0.28	0.42	0.51	581	1782	289.5	885.1
26	0.09	0.27	1452.89	14.83	0.31	0.38	0.55	375	1325	159.7	570.5
27	0.07	0.27	1319.67	14.81	0.32	0.39	0.40	387	1238	172.5	578.9
28	0.04	0.28	563.00	14.79	0.31	0.31	0.62	162	649	72.3	293.5
29	0.05	0.27	559.86	14.78	0.31	0.32	0.44	156	607	70.7	267.5
30	0.18	0.27	2533.75	14.57	0.27	0.42	0.41	754	2195	362.4	1026.7
31	0.17	0.27	2354.64	14.53	0.28	0.43	0.32	763	2229	361.9	1122.1
32	0.17	0.26	2062.96	14.53	0.28	0.42	0.41	638	1962	291.8	938.5
33	0.13	0.27	1614.83	14.56	0.31	0.41	0.34	559	1586	265.5	760.7
34	0.18	0.27	3210.56	14.60	0.27	0.43	0.42	990	2936	503.0	1473.9
35	0.16	0.26	1963.53	14.53	0.29	0.41	0.45	663	1925	307.7	913.7
36	0.16	0.26	1773.62	14.51	0.30	0.41	0.47	574	1902	301.1	943.5
37	0.18	0.28	4901.22	14.64	0.25	0.42	0.43	1439	4077	794.9	2218.5
38	0.12	0.27	2091.19	14.64	0.28	0.43	0.46	662	1945	319.2	948.1
39	0.18	0.28	3919.30	14.69	0.26	0.44	0.65	1217	3456	631.8	1804.2
40	0.09	0.28	2181.18	14.87	0.29	0.41	0.62	668	1936	315.1	933.3
41	0.10	0.28	2180.49	14.87	0.28	0.42	0.55	626	1905	318.2	965.4
42	0.13	0.26	1215.38	14.52	0.35	0.37	0.40	425	1389	190.2	637.7
43	0.10	0.28	2659.91	14.84	0.27	0.41	0.79	777	2290	345.8	1074.6
45	0.11	0.27	1541.36	14.59	0.31	0.40	0.38	485	1568	228.3	767.7
46	0.09	0.27	1428.63	14.60	0.30	0.41	0.38	454	1400	221.6	669.5

3.2 Model kinematics

Stars with apparent magnitudes within the limits $m_{min} = 13.7$ and $m_{max} = 15.5$ were selected from the model data. This magnitude range corresponds to the selection criteria imposed on the observed data sample, see Section 2.2. Model stars with total proper motions greater than 10 mas yr^{-1} (corresponding to $>380\,\mathrm{km\,s^{-1}}$ at a distance of the Galactic Centre) were excluded on the basis that such stars would be similarly excluded from any observed sample. The fraction of weight removed and number of stars removed in this way only amounted to a few per cent of the total weight and number of stars in each field. Bulge model stars were selected by requiring a distance $d > 6\,\mathrm{kpc}$.

The mean proper motion and proper motion dispersions in the latitude and longitude directions were computed along with their errors for all model stars in each field which obey the above selection criteria. The weights on model stars, γ_i, were used to compute these values.

We then tested whether the finite and discrete nature of the model data gives rise to uncertainties in the measured proper motion

Table 4. Proper motion (PM) dispersions in the longitude and latitude directions, σ_l, σ_b, and cross-correlation term C_{lb} for bulge stars in 45 OGLE-II fields. High-precision proper motion data for bulge stars were extracted from the OGLE-II proper motion catalogue (Sumi et al. 2004). N is the number of stars selected from each field. Field 44 was not used due to the low number of RCGs in this field.

Field	Field centre		PM dispersions (mas yr^{-1}) Longitude σ_l		Latitude σ_b		C_{lb}		
	$l(^\circ)$	$b(^\circ)$	Model	Observed	Model	Observed	Model	Observed	N
1	1.08	−3.62	3.02 ± 0.08	3.10 ± 0.02	2.46 ± 0.08	2.83 ± 0.02	0.01 ± 0.08	−0.13 ± 0.01	15 434
2	2.23	−3.46	3.02 ± 0.06	3.21 ± 0.02	2.68 ± 0.15	2.80 ± 0.02	0.12 ± 0.03	−0.14 ± 0.01	16 770
3	0.11	−1.93	3.19 ± 0.08	3.40 ± 0.01	2.64 ± 0.02	3.30 ± 0.02	0.02 ± 0.01	−0.08 ± 0.01	26 763
4	0.43	−2.01	3.26 ± 0.05	3.43 ± 0.02	2.80 ± 0.06	3.26 ± 0.01	0.01 ± 0.03	−0.11 ± 0.01	26 382
5	−0.23	−1.33	3.22 ± 0.15	3.23 ± 0.03	2.30 ± 0.07	3.00 ± 0.04	−0.01 ± 0.03	−0.04 ± 0.02	3145
6	−0.25	−5.70	3.26 ± 0.16	2.61 ± 0.02	2.42 ± 0.23	2.36 ± 0.03	−0.02 ± 0.13	−0.06 ± 0.01	7027
7	−0.14	−5.91	2.95 ± 0.15	2.70 ± 0.03	2.49 ± 0.12	2.43 ± 0.02	−0.15 ± 0.16	−0.05 ± 0.01	6236
8	10.48	−3.78	3.07 ± 0.09	2.80 ± 0.03	1.98 ± 0.14	2.29 ± 0.02	0.00 ± 0.09	−0.08 ± 0.01	5136
9	10.59	−3.98	3.28 ± 0.21	2.73 ± 0.02	2.03 ± 0.07	2.16 ± 0.03	−0.03 ± 0.07	−0.06 ± 0.01	5114
10	9.64	−3.44	3.30 ± 0.32	2.77 ± 0.02	2.89 ± 0.62	2.27 ± 0.02	0.09 ± 0.08	−0.07 ± 0.01	5568
11	9.74	−3.64	3.01 ± 0.20	2.84 ± 0.02	2.22 ± 0.29	2.32 ± 0.02	−0.08 ± 0.09	−0.10 ± 0.01	5369
12	7.80	−3.37	3.31 ± 0.10	2.66 ± 0.03	2.29 ± 0.06	2.31 ± 0.03	−0.09 ± 0.06	−0.08 ± 0.01	6035
13	7.91	−3.58	3.26 ± 0.18	2.66 ± 0.03	2.29 ± 0.12	2.24 ± 0.02	0.05 ± 0.02	−0.07 ± 0.01	5601
14	5.23	2.81	3.21 ± 0.05	2.97 ± 0.02	2.62 ± 0.13	2.60 ± 0.02	0.06 ± 0.04	0.04 ± 0.01	10 427
15	5.38	2.63	3.31 ± 0.12	3.02 ± 0.02	2.46 ± 0.07	2.64 ± 0.03	0.04 ± 0.04	−0.00 ± 0.01	8989
16	5.10	−3.29	3.19 ± 0.07	2.87 ± 0.02	2.23 ± 0.08	2.53 ± 0.02	0.03 ± 0.08	−0.12 ± 0.01	9799
17	5.28	−3.45	3.09 ± 0.09	2.81 ± 0.02	2.50 ± 0.07	2.42 ± 0.01	−0.01 ± 0.11	−0.12 ± 0.01	10 268
18	3.97	−3.14	3.20 ± 0.09	2.92 ± 0.02	2.48 ± 0.08	2.62 ± 0.02	0.02 ± 0.03	−0.13 ± 0.01	14 019
19	4.08	−3.35	3.06 ± 0.13	2.90 ± 0.02	2.49 ± 0.26	2.60 ± 0.02	0.01 ± 0.03	−0.17 ± 0.01	13 256
20	1.68	−2.47	3.12 ± 0.06	3.27 ± 0.01	2.66 ± 0.05	2.82 ± 0.01	0.07 ± 0.03	−0.12 ± 0.01	17 678
21	1.80	−2.66	3.12 ± 0.06	3.31 ± 0.02	2.57 ± 0.08	2.90 ± 0.02	−0.02 ± 0.03	−0.13 ± 0.01	17 577
22	−0.26	−2.95	3.17 ± 0.04	3.17 ± 0.02	2.46 ± 0.12	2.84 ± 0.02	0.01 ± 0.03	−0.01 ± 0.01	19 787
23	−0.50	−3.36	3.13 ± 0.17	3.15 ± 0.01	2.62 ± 0.10	2.84 ± 0.02	−0.02 ± 0.14	−0.04 ± 0.01	17 996
24	−2.44	−3.36	2.77 ± 0.04	2.96 ± 0.01	2.32 ± 0.10	2.48 ± 0.01	−0.04 ± 0.04	0.02 ± 0.01	16 397
25	−2.32	−3.56	2.76 ± 0.07	2.91 ± 0.01	2.47 ± 0.15	2.50 ± 0.01	−0.04 ± 0.03	0.02 ± 0.01	16 386
26	−4.90	−3.37	2.80 ± 0.17	2.68 ± 0.02	2.22 ± 0.04	2.17 ± 0.01	−0.00 ± 0.03	0.02 ± 0.01	13 099
27	−4.92	−3.65	2.78 ± 0.07	2.63 ± 0.02	2.19 ± 0.04	2.15 ± 0.01	−0.06 ± 0.02	0.03 ± 0.01	12 728
28	−6.76	−4.42	3.02 ± 0.11	2.63 ± 0.03	2.44 ± 0.36	2.12 ± 0.02	0.05 ± 0.06	−0.01 ± 0.01	8367
29	−6.64	−4.62	3.02 ± 0.21	2.66 ± 0.03	1.79 ± 0.14	2.09 ± 0.02	−0.00 ± 0.11	−0.02 ± 0.01	8108
30	1.94	−2.84	3.13 ± 0.07	3.04 ± 0.02	2.59 ± 0.11	2.70 ± 0.02	−0.04 ± 0.08	−0.12 ± 0.01	17 774
31	2.23	−2.94	3.08 ± 0.05	3.11 ± 0.02	2.68 ± 0.11	2.74 ± 0.01	0.08 ± 0.05	−0.12 ± 0.01	17 273
32	2.34	−3.14	3.10 ± 0.09	3.10 ± 0.02	2.56 ± 0.04	2.78 ± 0.01	0.11 ± 0.02	−0.13 ± 0.01	15 966
33	2.35	−3.66	2.82 ± 0.11	3.08 ± 0.02	2.57 ± 0.12	2.77 ± 0.02	0.07 ± 0.06	−0.14 ± 0.01	15 450
34	1.35	−2.40	3.18 ± 0.06	3.36 ± 0.02	2.62 ± 0.03	2.92 ± 0.01	0.04 ± 0.02	−0.11 ± 0.01	16 889
35	3.05	−3.00	3.05 ± 0.05	3.09 ± 0.02	2.59 ± 0.07	2.72 ± 0.02	0.08 ± 0.03	−0.14 ± 0.01	15 973
36	3.16	−3.20	3.00 ± 0.06	3.19 ± 0.02	2.95 ± 0.40	2.77 ± 0.02	−0.05 ± 0.08	−0.16 ± 0.01	14 955
37	0.00	−1.74	3.29 ± 0.04	3.29 ± 0.02	2.70 ± 0.04	3.04 ± 0.01	−0.01 ± 0.01	−0.05 ± 0.01	20 233
38	0.97	−3.42	3.01 ± 0.07	3.15 ± 0.01	2.60 ± 0.14	2.84 ± 0.02	0.07 ± 0.07	−0.12 ± 0.01	15 542
39	0.53	−2.21	3.22 ± 0.03	3.21 ± 0.01	2.69 ± 0.06	3.00 ± 0.01	0.01 ± 0.04	−0.07 ± 0.01	24 820
40	−2.99	−3.14	2.84 ± 0.04	2.84 ± 0.01	2.28 ± 0.07	2.47 ± 0.02	−0.09 ± 0.07	0.05 ± 0.01	13 581
41	−2.78	−3.27	2.86 ± 0.06	2.78 ± 0.01	2.60 ± 0.19	2.41 ± 0.02	−0.16 ± 0.07	0.04 ± 0.01	14 070
42	4.48	−3.38	3.07 ± 0.05	2.89 ± 0.02	2.44 ± 0.15	2.63 ± 0.02	0.02 ± 0.02	−0.15 ± 0.01	10 099
43	0.37	2.95	3.13 ± 0.06	3.17 ± 0.02	2.72 ± 0.10	2.87 ± 0.01	0.04 ± 0.07	0.02 ± 0.01	11 467
45	0.98	−3.94	3.02 ± 0.05	2.97 ± 0.04	2.42 ± 0.14	2.61 ± 0.04	0.06 ± 0.11	−0.13 ± 0.02	2380
46	1.09	−4.14	2.87 ± 0.08	2.90 ± 0.04	2.53 ± 0.21	2.67 ± 0.04	−0.03 ± 0.06	−0.16 ± 0.03	1803

dispersion values. We measured the intrinsic noise in the model by comparing the proper motion dispersions computed for four equivalent lines of sight through the model for each field. The spread of the proper motion dispersions for each field was then used as the estimate of the intrinsic noise in the model. The mean (median) value of these errors in the longitude and latitude directions are 0.08 (0.06) and 0.12 (0.097) mas yr^{-1}, respectively.

The statistical error for the proper motion dispersions in the longitude and latitude directions for each field were combined in quadrature with the error arising from the finite discrete nature of the model data to give the total error on the proper motion dispersions computed from the model.

4 COMPARISON BETWEEN THEORETICAL MODEL AND OBSERVED DATA

The observed and predicted proper motion dispersions for each of the OGLE-II fields are shown in Table 4. Fig. 8 shows the observed proper motion dispersions for each of the analysed OGLE-II fields plotted against the predicted model proper motion dispersions.

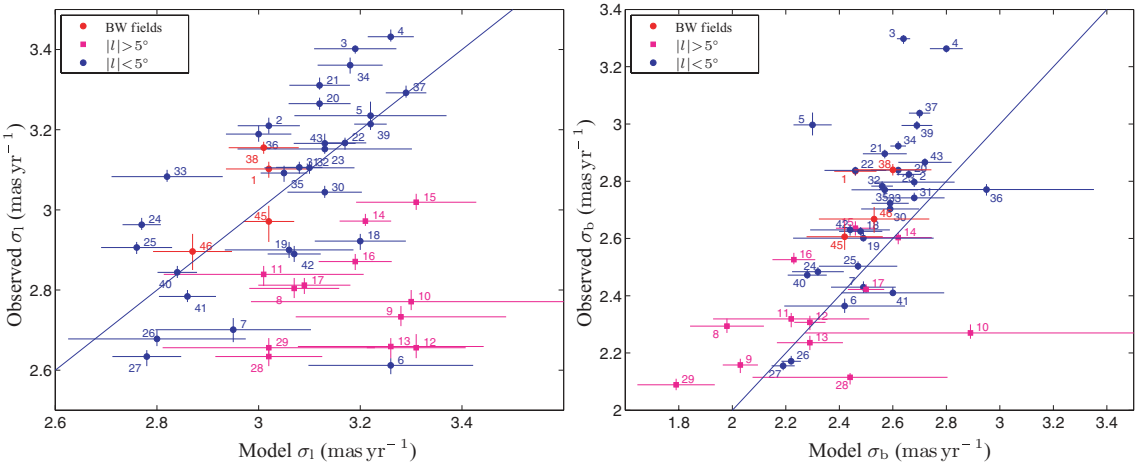

Figure 8. Comparison between observed and predicted proper motion dispersions for stars in the OGLE-II proper motion catalogue of Sumi et al. (2004). Left-hand panel: Proper motion dispersions in the galactic longitude direction, σ_l. The OGLE-II field number is indicated adjacent to each point, see also Fig. 1. Fields with galactic longitude $|l| > 5°$ are shown in magenta; fields within BW are shown in red; all other fields in blue. Right-hand panel: Proper motion dispersions in the galactic latitude direction, σ_b, shown with the same colour scheme.

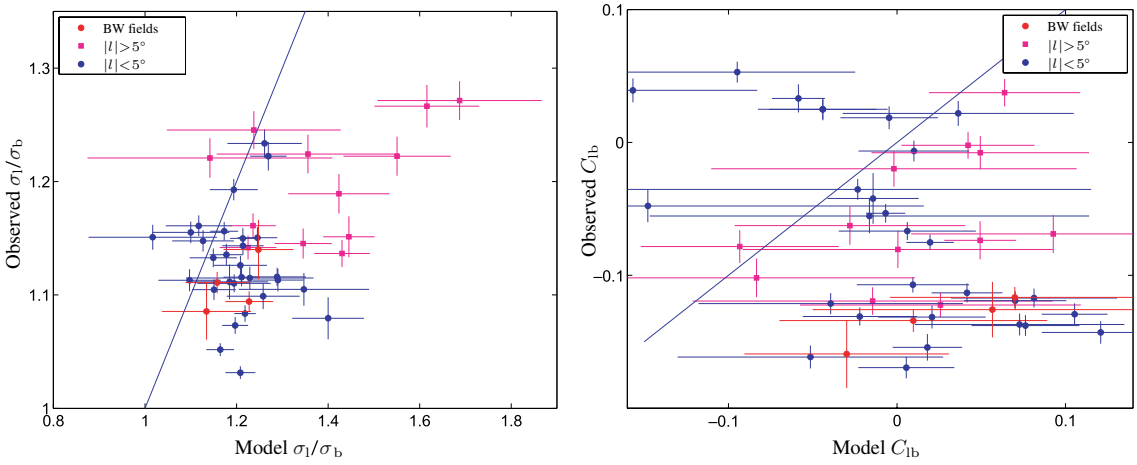

Figure 9. Left-hand panel: Ratio of proper motion dispersions $R = \sigma_l/\sigma_b$ for the observed OGLE-II proper motion data and model predictions. The model generally predicts more anisotropic motion, that is, $R > 1$ than is observed in the data. Right-hand panel: The cross-correlation term $C_{lb} = \sigma_{lb}/\sigma_l\,\sigma_b$.

Fig. 8 shows that the model predictions are in general agreement with observed proper motion dispersions for the OGLE-II fields. The model has been used previously to predict the proper motion dispersions of 427 star[1] entries observed by Spaenhauer et al. (1992) in a single 6 × 6-arcmin^2 field towards the bulge (Bissantz et al. 2004). The model value of σ_l in the previous analysis was in agreement with the observed value, yet the model and observed values of σ_b were significantly different. The 6 × 6-arcmin^2 field used by Spaenhauer et al. (1992) falls within the OGLE-II field number 45. The model prediction of σ_l for stars in OGLE field 45 is completely consistent with the measured value. The model prediction of σ_b shows a similar discrepancy to the previous analysis of Bissantz et al. (2004).

Fig. 9 shows the ratio $R = \sigma_l/\sigma_b$ and cross-correlation term $C_{lb} = \sigma_{lb}/(\sigma_l\sigma_b)$ computed using the model and observed data. Typically the model predicts more anisotropic motion with $R > 1$ than what is observed.

The model predictions for stellar kinematics in the latitude direction may be problematic. This is not surprising as the model is not well constrained towards the plane due to a lack of observational data because of the heavy dust extinction. The problem is currently under investigation. Similarly, the model predictions for σ_l degrade as l increases. This is because the model performance has been optimized for regions close to the Galactic Centre.

The significant difference between the observed proper motion dispersions of adjacent fields (e.g. fields 1 and 45) might hint at some fine-scale population effect, whereby a group of stars surviving the selection criteria have a significant and discrepant kinematic signature. Higher accuracy observations using the *HST* support this evidence of such population effects (Kozłowski et al. 2006).

No attempt has been made to account for the blending of flux inherent in the OGLE-II crowded-field photometry. It is certain that a fraction of stars in each OGLE-II field suffers from some degree of blending (Kozłowski et al. 2006). To investigate this effect, we checked one field covering the lens MACHO-95-BLG-37 ($l = 2.^\circ54,\ b = 3.^\circ33$, Thomas et al. 2005) from the *HST* proper motion survey of Kozłowski et al. (2006), which falls inside OGLE-II

[1]There are two repeated entries in table 2 of Spaenhauer et al. (1992).

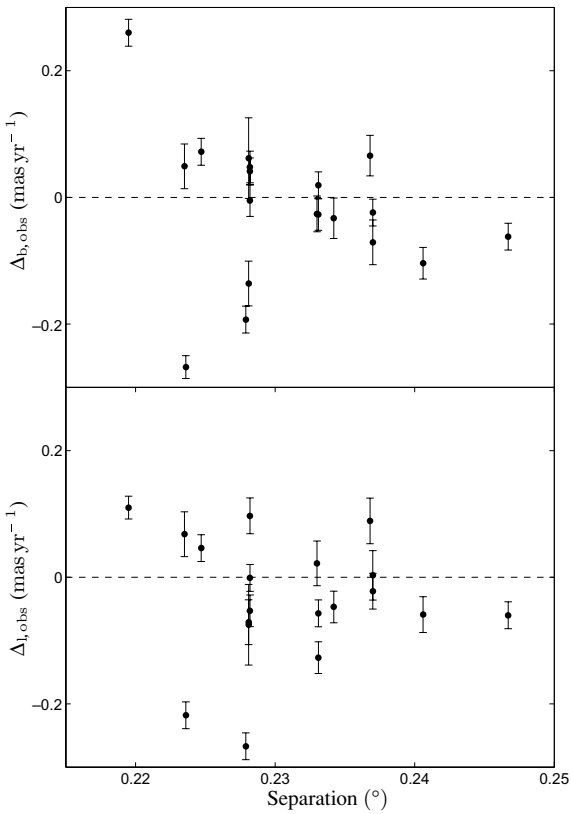

Figure 10. Difference between observed proper motion dispersions for pairs of fields with separations less than 0.°25 (corresponding to ≃40 pc at the Galactic Centre).

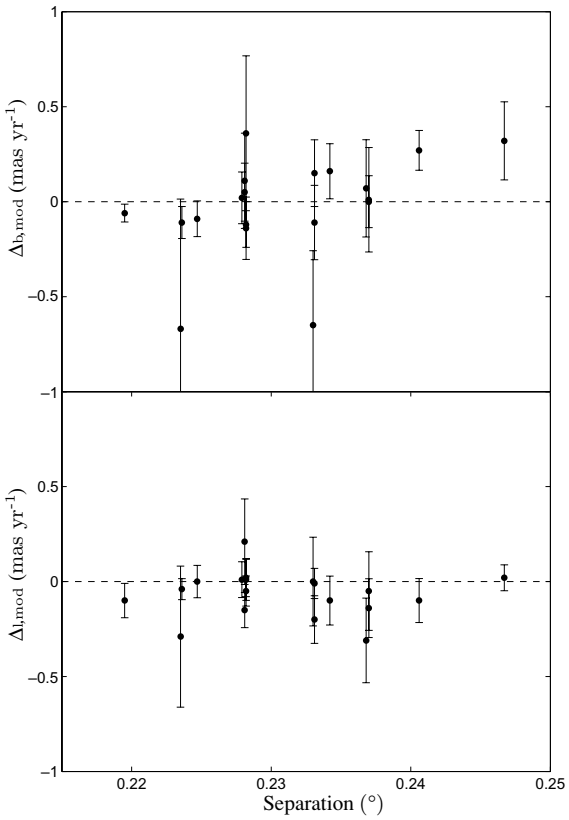

Figure 11. Difference between model proper motion dispersions for pairs of fields with separations less than 0.°25.

field number 2. *HST* images suffer much less blending, but the field of view is small, and so it has only a dozen or so clump giants. We derive a proper motion of $\sigma_l = 3.13 \pm 0.57$ mas yr^{-1}, and $\sigma_b = 2.17 \pm 0.40$ mas yr^{-1}. These values agree with our kinematics in field 2 within 0.2σ for σ_l and 1.6σ for σ_b. The errors in our proper motion dispersions are very small (∼km s^{-1} at a distance of the Galactic Centre), but it is likely that we underestimate the error bars on the observed data due to systematic effects such as blending.

4.1 Understanding the differences

We now seek to understand the cause of the differences between the model and the Milky Way, at least at a qualitative level. We first consider the possibility that the difference can be explained by some systematic effect. We compute the differences between observed proper motion dispersions of nearest fields for fields with separations less than 0.°25. No pair of fields is used twice, and the difference $\Delta = \sigma_i - \sigma_j$ is always plotted such that $|b_i| \geqslant |b_j|$. $\Delta_{l,obs}$ and $\Delta_{b,obs}$ denote the difference in observed proper motion dispersions between adjacent fields in the longitude and latitude directions, respectively. The equivalent quantities predicted from the model are denoted $\Delta_{l,mod}$ and $\Delta_{b,mod}$. In Fig. 10 we see that the deviations $\Delta_{l,obs}$ and $\Delta_{b,obs}$ scatter about 0, but have a quite broad distribution in both the l and b directions, with several fields inconsistent with zero difference at 1σ (defined as the sum in quadrature of the uncertainties of the corresponding quantities of the two fields under comparison). Several deviations are as large as 0.2 mas yr^{-1} (corresponding to ≃8 km s^{-1} at the Galactic Centre) and many σ away from zero. In view of the fact that these differences have mean close to zero, it is possible that these deviations are due to some systematic effect rather than to intrinsic substructure in the Milky Way. We return to this point briefly in the discussion.

In the case of the model uncertainties, however, Fig. 11 shows that in most cases the differences $\Delta_{l,mod}$ and $\Delta_{b,mod}$ are consistent with zero at the 1σ level, indicating that these error estimates are robust.

We now seek to explore the correlations of the residuals with properties of the model. We plot residuals $\delta_{l,b} = (\sigma_{mod} - \sigma_{obs})$, where σ_{mod} and σ_{obs} are the model and observed proper motion dispersions in the corresponding Galactic coordinate. The error bar length is $(u_{mod}^2 + u_{obs}^2)^{1/2}$ where u_{mod} and u_{obs} are the uncertainties in the model and observed proper motion dispersions, respectively. Plotting these quantities as a function of l, we note that there is no significant correlation, but that the largest deviations in the latitude proper motion dispersion occur close to $l = 0$, see Fig. 12. In plotting $\delta_{l,b}$ as a function of b, the reason which becomes evident is that the fields closest to the mid-plane have the largest δ_b, see Fig. 13. The density distribution in this region is uncertain due to presence of dust and the large extinction corrections required. This may explain why the residuals of σ_b seem to correlate more with b than those of σ_l. We note that the σ_l residuals also seem to have some dependence on b. A possible explanation is that there is some additional effect due to dust which has not been accounted for.

5 DISCUSSION

RCG stars in the dense fields observed by the OGLE-II microlensing survey can be used as tracers of the bulge density and motion over a large region towards the Galactic Centre. The proper

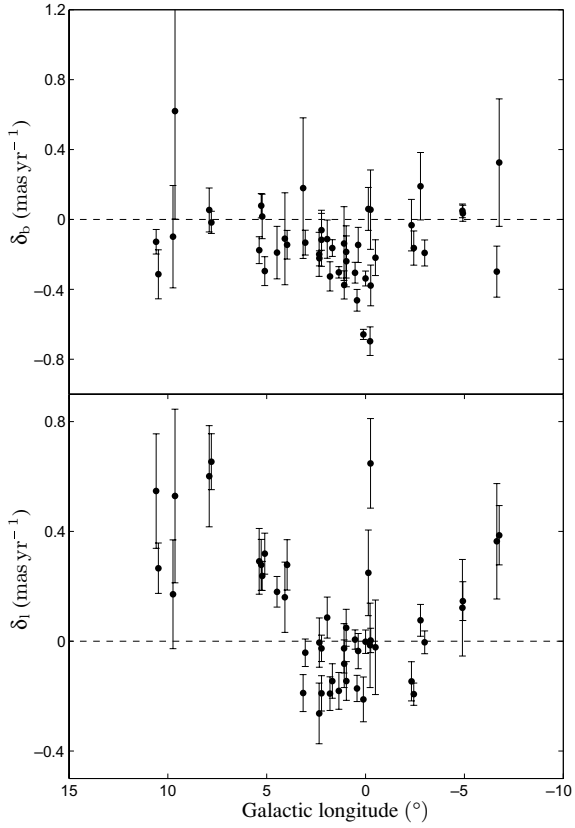

Figure 12. Residuals $\delta_{l,b} = (\sigma_{mod} - \sigma_{obs})$ (see text), plotted against longitude, *l*.

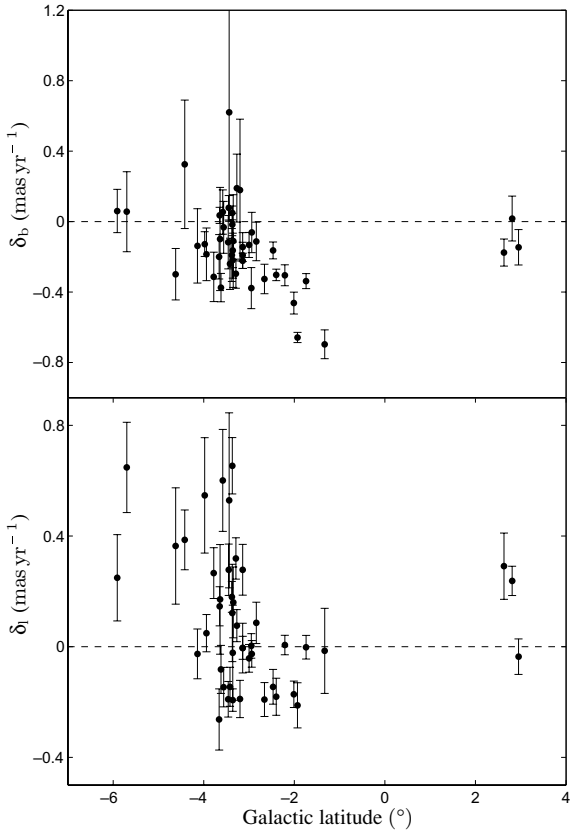

Figure 13. Residuals $\delta_{l,b} = (\sigma_{mod} - \sigma_{obs})$ (see text), plotted against latitude, *b*.

motion dispersions of bulge RCG stars in the OGLE-II proper motion catalogue of Sumi et al. (2004) were calculated for 45 OGLE-II fields. The kinematics derived from the ground-based OGLE-II data were found to be in agreement with *HST* observations in two fields from Kozłowski et al. (2006). It is reassuring that the results presented here are consistent with those derived from the higher resolution *HST* data, despite possible selection effects and blending.

The observed values of σ_l and σ_b were compared to predictions from the made-to-measure stellar dynamical model of Debattista et al. (in preparation). In general, the model gives predictions qualitatively similar to observed values of σ_l and σ_b for fields close to the Galactic Centre. The model is in agreement with observed OGLE-II data in the direction previously tested by Bissantz et al. (2004). Using the definition of De Lorenzi et al. (2007), the effective number of particles in the model used here is 3986. This relatively low number results in large errors on the model proper motion dispersions and we therefore recommend regarding interpretations based on this model with some caution. An improved model with a larger number of particles (the recent study by De Lorenzi et al. (2007) has an effective particle number $\sim 10^6$) will decrease the errors on the model predictions and allow a more useful comparison between model and observed proper motion dispersions.

The OGLE-II fields mostly extend over $\sim 17^\circ$ in longitude and about 5° in latitude across the Galactic bulge region and can therefore provide a more powerful set of constraints on stellar motions predicted by galactic models. The high-accuracy proper motion data for the 45 fields and those obtained with *HST* (Kozłowski et al. 2006) can be used as direct input in the made-to-measure method to construct a better constrained dynamical model of the Milky Way.

The statistical errors of our proper motion dispersions are small ($\sim$ km s^{-1}), but systematic uncertainties (e.g. due to incorrect dust-extinction treatment) which were not included in the analysis may be significant. Nevertheless, it is interesting to note that there appears to be significant difference between the observed proper motion dispersions of adjacent fields (e.g. fields 1 and 45). This might hint at some fine-scale population effect, where the kinematics of the bulge may be not in total equilibrium (e.g. due to a small accretion event). Higher accuracy observations using the *HST* may provide further evidence of such population effects. We note that Rich et al. (2006) suggest the possible existence of cold structures using data from a radial velocity survey of Galactic bulge M giant stars although their conclusion could be strengthened by a larger sample of stars.

The OGLE-II proper motion catalogue (Sumi et al. 2004) for millions of bulge stars is still somewhat underexplored. For example, it will be interesting to explore the nature of the high proper motion stars ($\mu > 10$ mas yr^{-1}) and search for wide binaries in the catalogue. Some exploration along these lines is under way.

ACKNOWLEDGMENTS

We thank Drs Vasily Belokurov, Wyn Evans and Martin Smith for helpful discussions, and the anonymous referee for his/her helpful suggestions.

NJR acknowledges financial support by a PPARC PDRA fellowship. This work was partially supported by the European Community's Sixth Framework Marie Curie Research Training Network Programme, Contract No. MRTN-CT-2004-505183 'ANGLES'. VPD is supported by a Brooks Prize Fellowship at the University

of Washington and receives partial support from NSF ITR grant PHY-0205413.

REFERENCES

Alcock C., Allsman R. A., Alves D. R. et al., 2000, ApJ, 541, 734
Aubourg E., Bareyre P., Brehin S. et al., 1993, Nat, 365, 623
Babusiaux C., Gilmore G., 2005, MNRAS, 358, 1309
Benjamin R. A. et al., 2005, ApJ, 630, L149
Binney J., Gerhard O., Spergel D., 1997, MNRAS, 288, 365
Bissantz N., Gerhard O., 2002, MNRAS, 330, 591
Bissantz N., Debattista V. P., Gerhard O., 2004, ApJ, 601, L155
Bond I. A. et al., 2001, MNRAS, 327, 868
De Lorenzi F., Debattista V., Gerhard O., Sambhus N., 2007, MNRAS, 376, 71
Dwek E. et al., 1995, ApJ, 445, 716
Eisenhauer F. et al., 2005, ApJ, 628, 246
Evans N. W., Belokurov V., 2002, ApJ, 567, L119
Eyer L., Woźniak P. R., 2001, MNRAS, 327, 601
Gerhard O., 2002, in Da Costa G. S., Jerjen H., eds, ASP Conf. Ser. Vol. 273, The Dynamics, Structure & History of Galaxies: A Workshop in Honour of Professor Ken Freeman. Astron. Soc. Pac., San Francisco, p. 73
Girardi L., Salaris M., 2001, MNRAS, 323, 109
Kozłowski S., Woźniak P. R., Mao S., Smith M. C., Sumi T., Vestrand W. T., Wyrzykowski L., 2006, MNRAS, 370, 435
Lupton R. H., Gunn J. E., Griffin R. F., 1987, AJ, 93, 1114
Nikolaev S., Weinberg M. D., 1997, ApJ, 487, 885
Nishiyama S. et al., 2005, ApJ, 621, L105
Nishiyama S. et al., 2006, ApJ, 647, 1093
Percival S. M., Salaris M., 2003, MNRAS, 343, 539
Rattenbury N. J., Mao S., Sumi T., Smith M. C., 2007, MNRAS, in press (doi:10.1111/j.1365-2966.11843.x)
Rich M. R., Reitzel D. B., Howard C. D., Zhao H., 2007, ApJ, 658, L29
Rocha L., Velho L., Carvalho P. C. P., 2002, in Goncalves L. M. G., Musse S. M., eds, XV Brazilian Symposium on Computer Graphics and Image Processing. IEEE Computer Soc., p. 1530, (http://computer.org/proceedings/sibgrapi/1846/18460099abs.htm)
Salaris M., Percival S., Brocato E., Raimondo G., Walker A. R., 2003, ApJ, 588, 801
Spaenhauer A., Jones B. F., Whitford A. E., 1992, AJ, 103, 297
Spergel D. N., Malhotra S., Blitz L., 1996, in Minniti D., Rix H. W., eds, Proc. ESO/MPA Workshop, Spiral Galaxies in the Near-IR. Springer-Verlag, Berlin, p. 128
Stanek K. Z., Udalski A., Szymanski M., Kaluzny J., Kubiak M., Mateo M., Krzeminski W., 1997, ApJ, 477, 163
Stanek K. Z., Kaluzny J., Wysocka A., Thompson I., 2000, Acta Astron., 50, 191
Sumi T., 2004, MNRAS, 349, 193
Sumi T. et al., 2003a, ApJ, 591, 204
Sumi T., Eyer L., Woźniak P. R., 2003b, MNRAS, 340, 1346
Sumi T. et al., 2004, MNRAS, 348, 1439
Syer D., Tremaine S., 1996, MNRAS, 282, 223
Thomas C. L. et al., 2005, ApJ, 631, 906
Udalski A., 2000, ApJ, 531, L25
Udalski A., Zebrun K., Szymanski M., Kubiak M., Pietrzynski G., Soszynski I., Wozniak P., 2000, Acta Astron., 50, 1
Unavane M., Gilmore G., 1998, MNRAS, 295, 145
Zhao G., Qiu H. M., Mao S., 2001, ApJ, 551, L85

This paper has been typeset from a TEX/LATEX file prepared by the author.